Electronic Supplementary Material (ESI) for Physical Chemistry Chemical Physics.

Supporting Information for

The role of solvation models on the computed absorption and emission spectra: the case of fireflies oxyluciferin

Cristina Garcia-Iriepa[a], Madjid Zemmouche[a], Miguel Ponce-Vargas[a,b] and Isabelle Navizet[a]**

[a] *Université Paris-Est, Laboratoire Modélisation et Simulation Multi Échelle, MSME UMR 8208 CNRS, UPEM, 5 bd Descartes, 77454 Marne-la-Vallée, France*

[b] *Institut de Chimie Moléculaire de Reims, CNRS UMR 7312, Université de Reims Champagne-Ardenne, BP 1039, 51687 Reims, France*

Table of contents

1. MD and QM/MM computational details.

The TIP3P model[1] was used for solvating the chromophore within an octahedral box of water molecules, ensuring a solvent shell of at least 10 Å around the molecule, corresponding to around 900 water molecules. Then, after minimization, the system was heated from 100 to 300 K in 20 ps. Finally a production run of 10 ns has been performed with a 2 fs time step, under NPT conditions (300 K and 1 atm) and using periodic boundary conditions. The pressure and temperature were assured by the Berendsen algorithm.[2] Regarding the chromophore, parameters obtained from the QM calculation in gas phase were used as a first approximation. Then, a reparametrization has been performed following the already published procedure:[3] for each set of parameters, a corresponding 10 ns MD was performed, 100 snapshots were extracted, and the QM/MM absorption (emission) spectra were simulated. New parameters were adjusted from the QM/MM calculation, and the process was performed with the new set of parameters until reaching the spectral shape convergence between the previous and the next simulated spectra.

2. Benchmark of different basis sets.

A benchmark of different basis sets has been performed using the B3LYP functional for the phenolate-keto derivative as a representative compound both using PCM (Table S1) and with QM/MM methods (two snapshots which transition energy matches with the maximum absorption and emission wavelengths have been selected) (Table S2). By analyzing the data we observe that the differences between the absorption and emission energies computed with the smallest 6-311G(2d,p) and the larger basis sets are ≤ 0.05 eV, which is within the method error. However, using the smallest 6-311G(2d,p) basis set the calculation time is reduced almost 10 times compared to the following in size 6-311G+(2d,p) basis set. For this reason, the choice of the 6-311g(2d,p) basis set seems reasonable.

Table S1. Computed and experimental absorption and emission energies (in eV) of phenolate-keto in water (LR-PCM) with different basis set. The computational cost to obtain both the absorption and emission energies is evaluated as the CPU hours needed for optimization and vertical transition energies calculation.

Basis set	$E_{abs}^{theor.}$	$E_{abs}^{exp.}$[a]	$E_{emi}^{theor.}$	$E_{emi}^{exp.}$[a]	Comp. cost (CPU h)
6-311G(2d,p)	2.50	2.57	2.09	1.93	11
6-311+G(2d,p)	2.45		2.06		172
6-311++G(2df,2pd)	2.45		2.06		200
aug-cc-pVTZ	2.45		2.06		1234

[a] *Ref.* [4]

Table S2. Computed and experimental absorption and emission energies (in eV) of phenolate-keto in explicit water with different basis set. One representative snapshot from the dynamic was used for the absorption calculated at the QM/MM level and another snapshot for the emission at the QM/MM level. The computational cost to obtain the absorption (resp. the emission energies) is evaluated as the CPU hours needed for optimization and vertical transition energies calculation. The addition of the two CPU is reported in the last column to be compared to the one of Table S1.

Basis set	$E_{abs}^{theor.}$	$E_{abs}^{exp.a}$	$E_{emi}^{theor.}$	$E_{emi}^{exp.a}$	Comp. cost (CPU h)
6-311G(2d,p)	2.55	2.57	2.05	1.93	19
6-311+G(2d,p)	2.54		2.05		177
6-311++G(2df,2pd)	2.54		2.05		215

[a] *Ref.* 4

3. Benchmark of different functionals.

Different functionals were also tested. We have tested hybrid functionals: B3LYP,[5,6] PBE0,[7,8] M06,[9] M06-2X,[9] with resp. 20%, 25%, 27%, 54% of Hartree-Fock exchange, and hybrid functional with the long-range correction: CAM-B3LYP. All values are in the range of 0.3 eV. The more the percentage of Hartree-Fock exchange, the bigger the predicted transition energy is and the bigger the oscillator strength. We have chosen the most common used functional B3LYP for the further study as it is also the one that gives the emission energy closest to the experimental value (1.93 eV).

Table S3. Computed absorption and emission energies and oscillator strengths (*f*) of phenolate-keto in water (LR-PCM) using the 6-311G(2d,p) basis set with different DFT functionals.

Functional	**LR-PCM**		**Gas Phase**	
	$E_{abs}^{theor.}$ **eV (nm)**	f	$E_{abs}^{theor.}$ **eV (nm)**	f
B3LYP	2.50 (496)	0.72	2.60 (476)	0.59
PBE0	2.56 (484)	0.75	2.66 (466)	0.62
M06	2.54 (488)	0.73	2.63 (471)	0.61
M06-2X	2.70 (460)	0.87	2.76 (450)	0.79
CAM-B3LYP	2.70 (460)	0.87	2.77 (448)	0.79

4. Charge transfer analysis

The B3LYP functional and the 6-311G(2d, p) atomic basis set were applied for geometry optimizations, frequency calculations, and electronic transitions. In order to reproduce the solvation effects of water, the Polarizable Continuum Model (PCM) was taken into account.

The amount of charge transfered (q^{CT} in e) defined as

$$q^{CT} = \sum_i q_i^+ = -\sum_i q_i^-$$

and the CT distance (d_{CT} in Å) have been calculated for the absorption according to the methodology proposed by Le Bahers and coworkers.[10,11]

The amount of charge transferred (q^{CT}) computed for phenol-keto and phenol-enolate and their analogues are the largest one, in line with the largest charge difference of the thiazole moiety computed for these derivatives (see absolute value of $\Delta_{1\rightarrow0}q^{th}$ in Table 2). Moreover, for the rest of the derivatives lower, but similar between them, charge transferred amount values were found. However, the d_{CT} values for phenol-enol and its analogues are smaller than the one found for the other derivatives, indicating delocalization of the charge transfer, that is, a small spatial transfer. This is in line with the low charge difference of the thiazole moiety computed for them ($\Delta_{1\rightarrow0}q^{th}$ in Table 2). In addition, for phenolate-enol, phenolate-keto and their analogues the q^{CT} obtained are similar to the one of phenol-enol but the d_{CT} values are larger, indicating a significant spatial character of the charge transfer, in agreement with the intermediate $\Delta_{1\rightarrow0}q^{th}$ computed (Table 2). It should be noted that for phenolate-enol, the d_{CT} is quite small indicating a delocalization of the charge transferred. However, the $\Delta_{1\rightarrow0}q^{th}$ calculated is intermediate. We postulate that phenolate-enolate is not a push-pull molecule (*i.e.* donor-πbridge-acceptor) as two negative charges are placed in each side of the molecule and so, the use of this methodology indicated for push-pull molecules could not be suitable for this derivative.

Table S4. Charge transfer (e) and charge transfer distance d_{CT} (Å) for the studied systems.

	Absorption		Emission	
	q^{CT} (e)	d_{CT} (Å)	q^{CT} (e)	d_{CT} (Å)
Phenol-enol	0.460	1.247	0.385	0.978
Phenol-OMe	0.469	0.982	0.399	0.704
OMe-Enol	0.479	1.823	0.398	1.509
Phenol-keto	0.611	3.732	0.540	3.534
Phenol-cycle	0.600	3.502	0.578	3.118
Phenol-enolate	0.504	3.085	0.445	2.959
OMe-enolate	0.504	3.136	0.444	3.005
Phenolate-enol	0.470	3.253	0.419	3.023
Phenolate-OMe	0.472	3.276	0.422	3.055
Phenolate-keto	0.397	2.403	0.421	2.657
Phenolate-cycle	0.408	2.475	0.429	2.718
Phenolate-enolate	0.470	0.995	0.409	1.462

In order to visualize the electronic density redistribution and the possible intramolecular charge transferred (CT) we calculate the difference between the total densities of the excited and ground states (EDD) provided by TD-DFT calculations. The isosurfaces have been plotted with the Chemcraft code,[12] considering a contour threshold of 0.004 a.u.

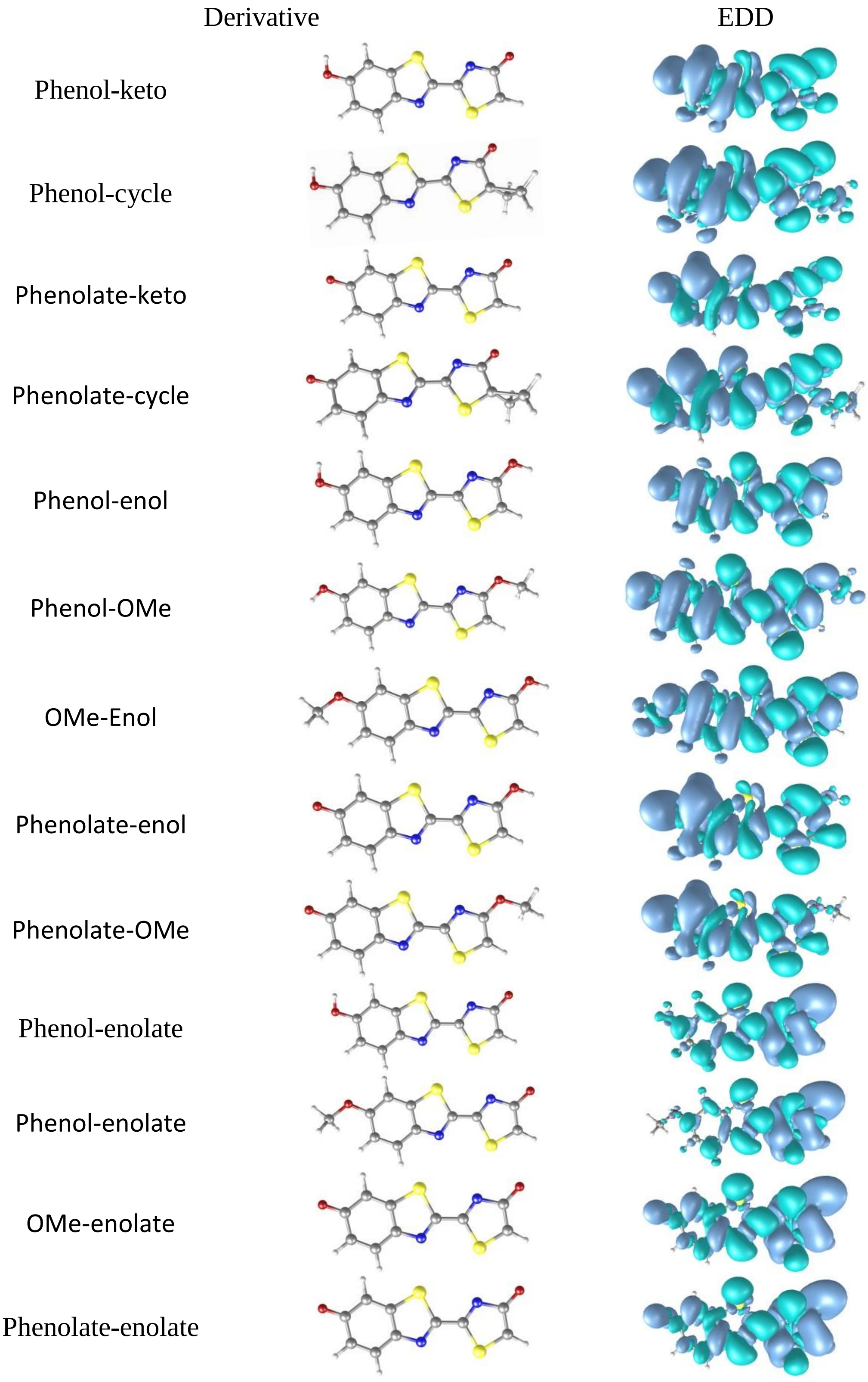

Figure S1. Electronic Density Difference plots for the studied systems. Turquoise and blue colors indicate charge accumulation and depletion, respectively. A contour threshold of 0.004 a.u. has been considered.

5. Natural transition orbitals.

The natural transition orbitals (NTO) have been obtained in gas phase and with the LR-PCM formalisms for all the oxyluciferin possible forms for both the absorption (Table S3) and emission (Table S4). We observe that in general the electron density of the NTO computed in gas phase and within the LR-PCM approach are quite similar except for phenol-keto. In this case, there is a big difference between gas phase and LR-PCM. In particular for phenol-keto, after optimization on the first excited state within the LR-PCM formalism we get that the most stable excited state characterized by an optically bright π,π* transition (also found for the other derivatives both in the gas phase and with LR-PCM). However, in the gas phase this optically bright state is not the most stable one but, the one resulting from the dark n,π* transition, with the n orbital being the one of the oxygen atom of the keto moiety (Figure S1A) that is over-stabilized. For this reason, we cannot give the emission energy value for phenol-keto computed in gas phase.

Table S5. Natural transition orbitals (NTO) computed for the absorption both in gas phase and within the LR-PCM formalism.

	Absorption NTO			
	Gas Phase		LR-PCM	
	HOMO	LUMO	HOMO	LUMO
Phenol_keto	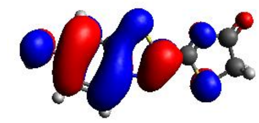	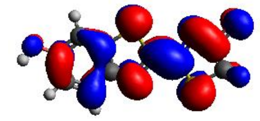	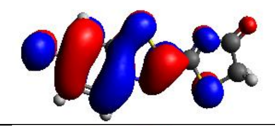	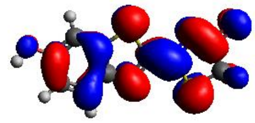
Phenolate_keto	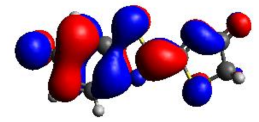	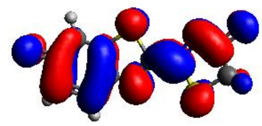	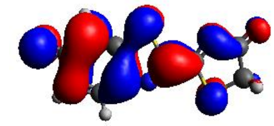	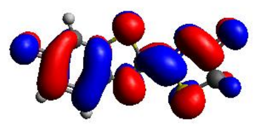
Phenol_enol	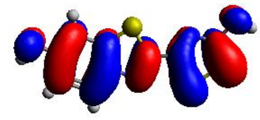	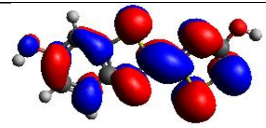	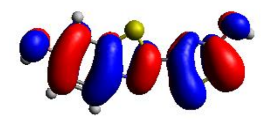	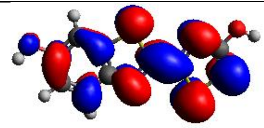
Phenolate_enol	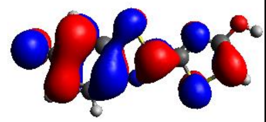	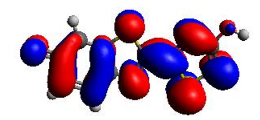	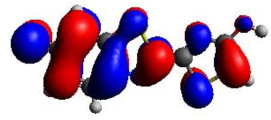	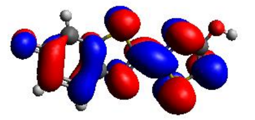
Phenol_enolate	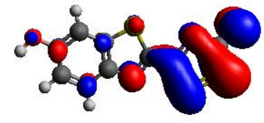	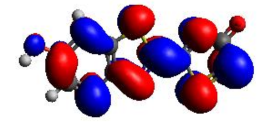	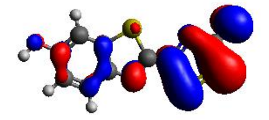	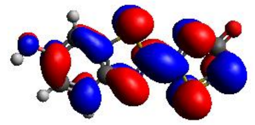
Phenolate_enolate	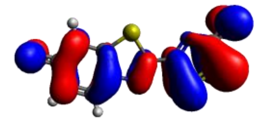	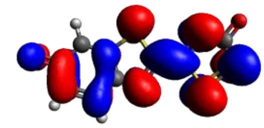	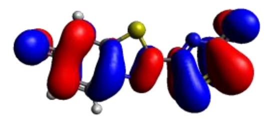	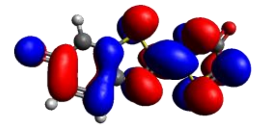

Table S6. Natural transition orbitals (NTO) computed for the emission both in gas phase and within the LR-PCM formalism. In blue is given the n,π* transition in gas phase for phenol-keto. This transition is over-stabilized compared to the expected π,π* transition seen for other derivatives.

	Emission NTO			
	Gas Phase		LR-PCM	
	HOMO	LUMO	HOMO	LUMO
Phenol_keto	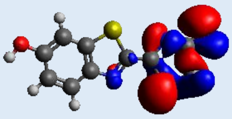	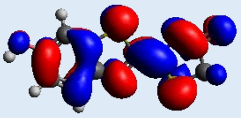	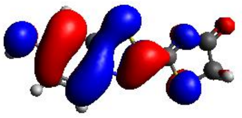	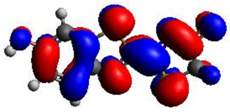
Phenolate_keto	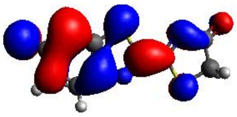	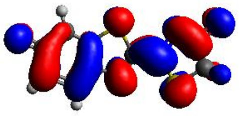	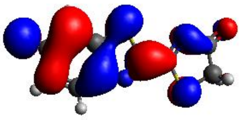	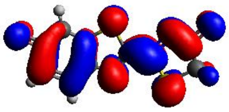
Phenol_enol	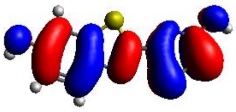	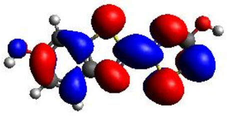	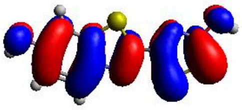	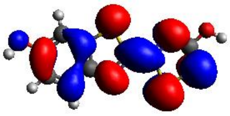
Phenolate_enol	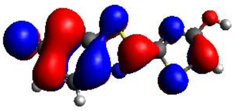	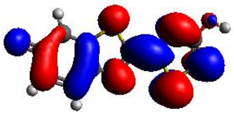	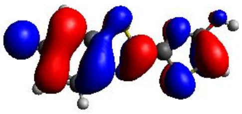	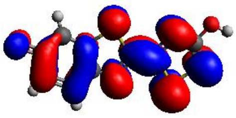
Phenol_enolate	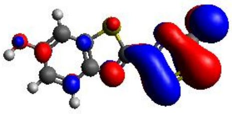	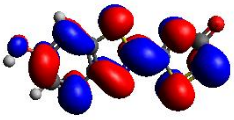	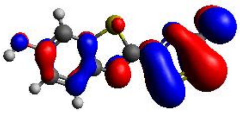	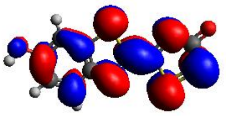
Phenolate_enolate	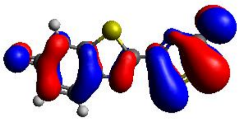	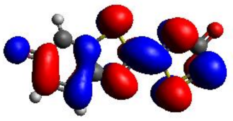	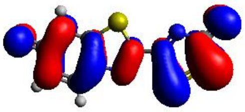	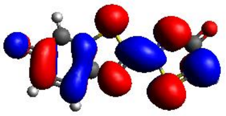

6. Comparison of the spectra computed in GP, LR-PCM and QM/MM.

The absorption spectra have been simulated in all cases as a convolution of gaussian functions using a full-width at half-maximum of 0.2 eV. In gas phase and within the LR-PCM method, the first three electronic transitions of the equilibrium ground state geometry (the minimum geometry of the ground state) have been considered whereas, for the spectra simulated with QM/MM methods in explicit water, 100 snapshots issued from the classical dynamic were used and for each the first three electronic transitions were calculated. The corresponding spectrum results from the convolution of the 100 snapshots.

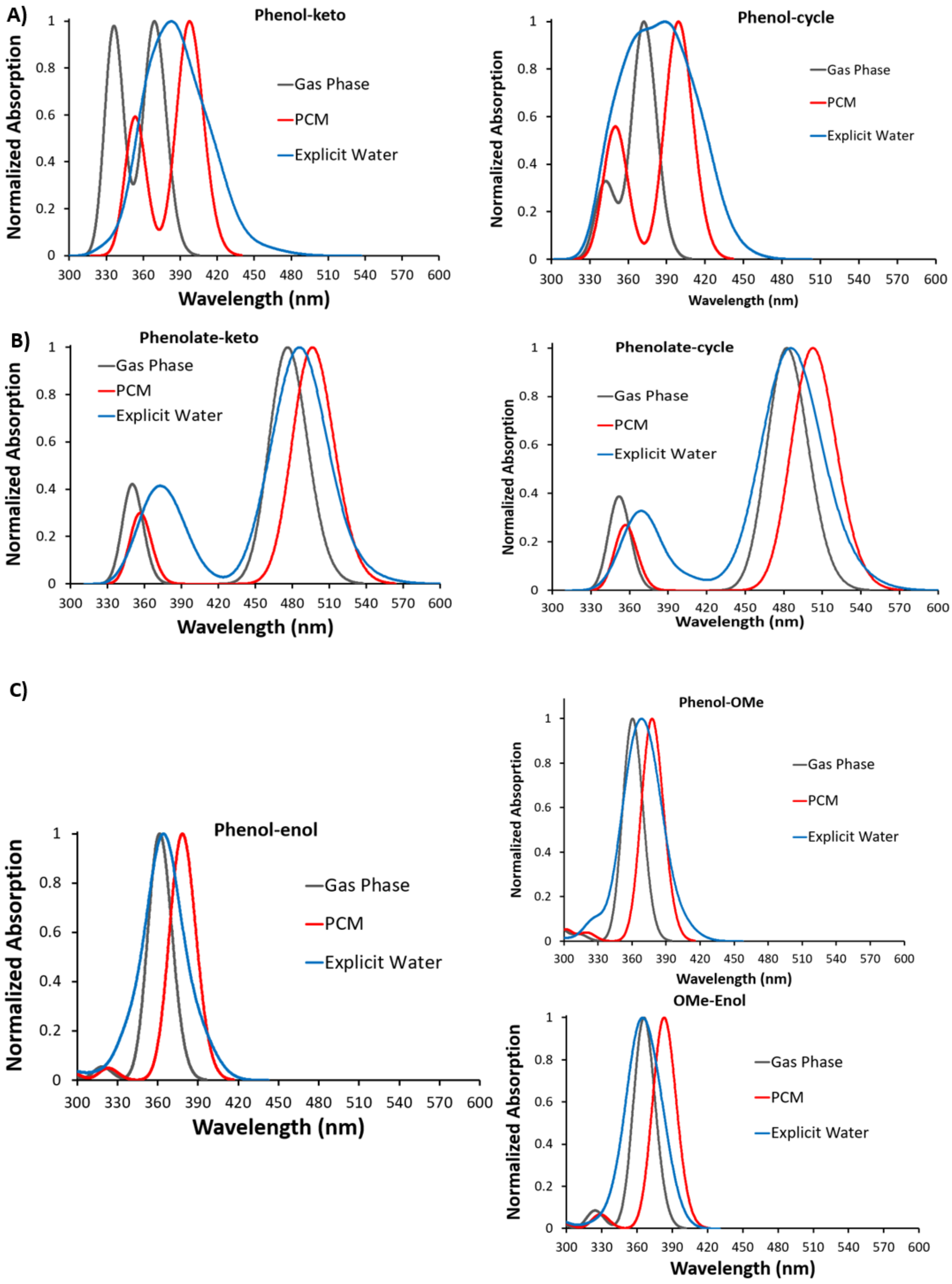
A)
Phenol-keto
Phenol-cycle
B)
Phenolate-keto
Phenolate-cycle
C)
Phenol-enol
Phenol-OMe
OMe-Enol
Gas Phase
PCM
Explicit Water
Normalized Absorption
Wavelength (nm)
0
0.2
0.4
0.6
0.8
1
300
330
360
390
420
450
480
510
540
570
600

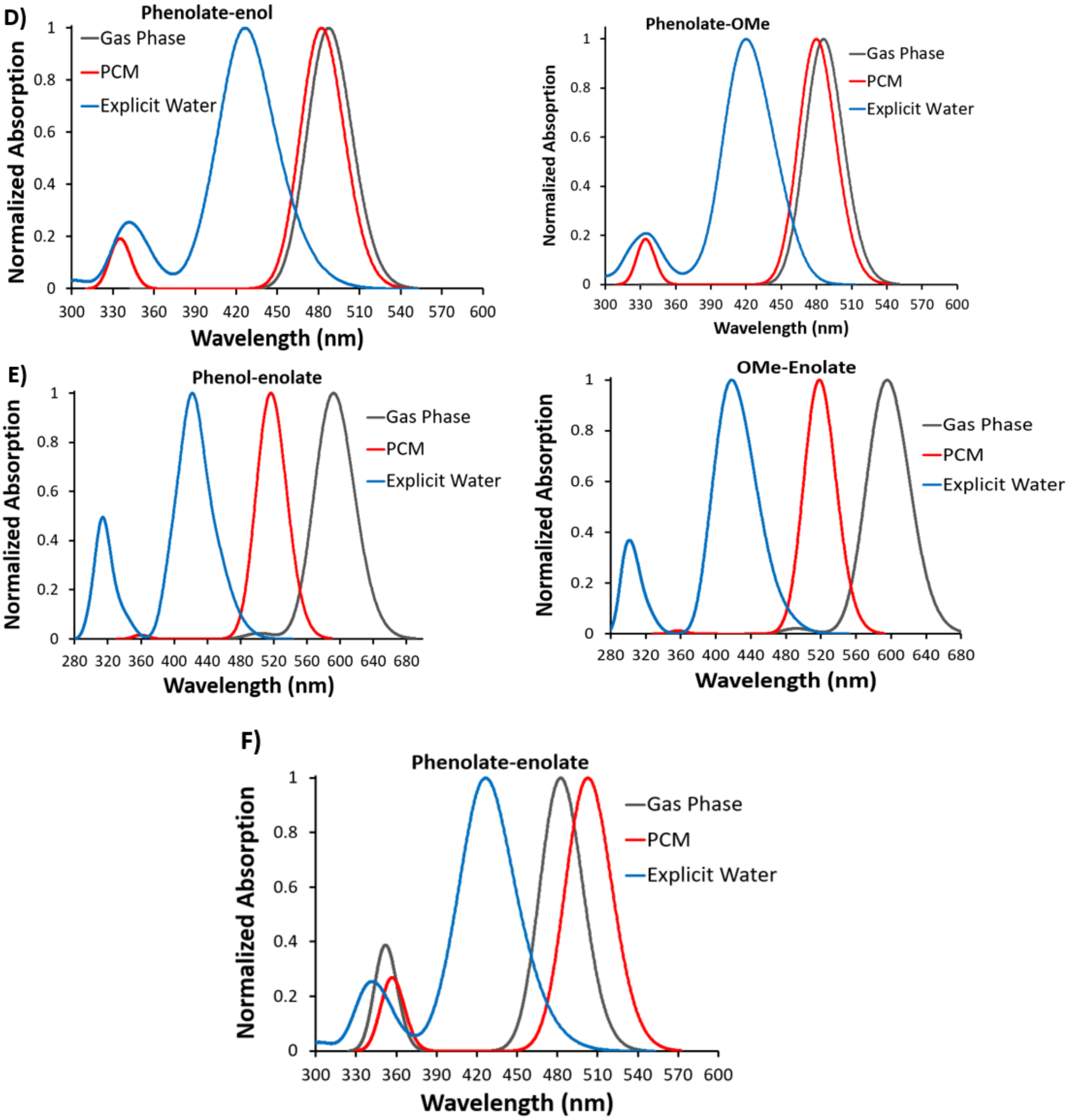

Figure S2. Comparison of the absorption spectra computed in the gas phase, within the LR-PCM formalism and QM/MM considering 100 MD snapshots for A) phenol-keto and its analogue, B) phenolate-keto and its analogue, C) phenol-enol and its analogues, D) phenolate-enol and its analogue, E) phenol-enolate and its analogue and F) phenolate-enolate.

As for the absorption, the emission spectra have been also simulated in the gas phase, within the LR-PCM formalism and with the QM/MM method. It has to be noticed that for phenol-keto and its analogue we do not give the emission spectra simulated in the gas phase (Figure S2A), as the n,π* transition is over-stabilized with respect to the π,π* transition responsible of the emission, as explained in section 4.

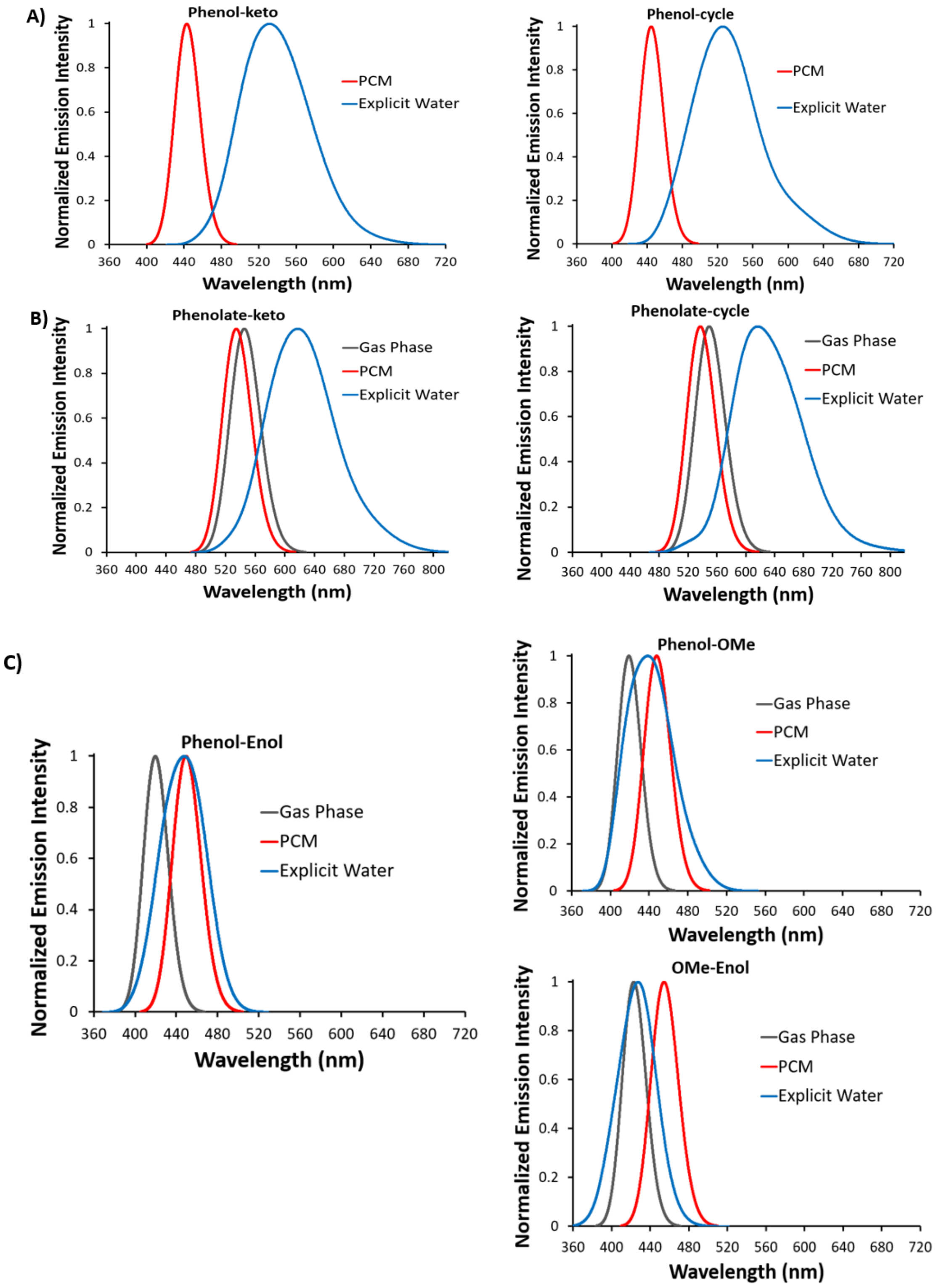
A)
Phenol-keto
Normalized Emission Intensity
1
0.8
0.6
0.4
0.2
0
360
400
440
480
520
560
600
640
680
720
Wavelength (nm)
PCM
Explicit Water
Phenol-cycle
Normalized Emission Intensity
Wavelength (nm)
PCM
Explicit Water
B)
Phenolate-keto
Normalized Emission Intensity
360 400 440 480 520 560 600 640 680 720 760 800
Wavelength (nm)
Gas Phase
PCM
Explicit Water
Phenolate-cycle
Normalized Emission Intensity
360 400 440 480 520 560 600 640 680 720 760 800
Wavelength (nm)
Gas Phase
PCM
Explicit Water
C)
Phenol-Enol
Normalized Emission Intensity
Wavelength (nm)
Gas Phase
PCM
Explicit Water
Phenol-OMe
Normalized Emission Intensity
Wavelength (nm)
Gas Phase
PCM
Explicit Water
OMe-Enol
Normalized Emission Intensity
Wavelength (nm)
Gas Phase
PCM
Explicit Water

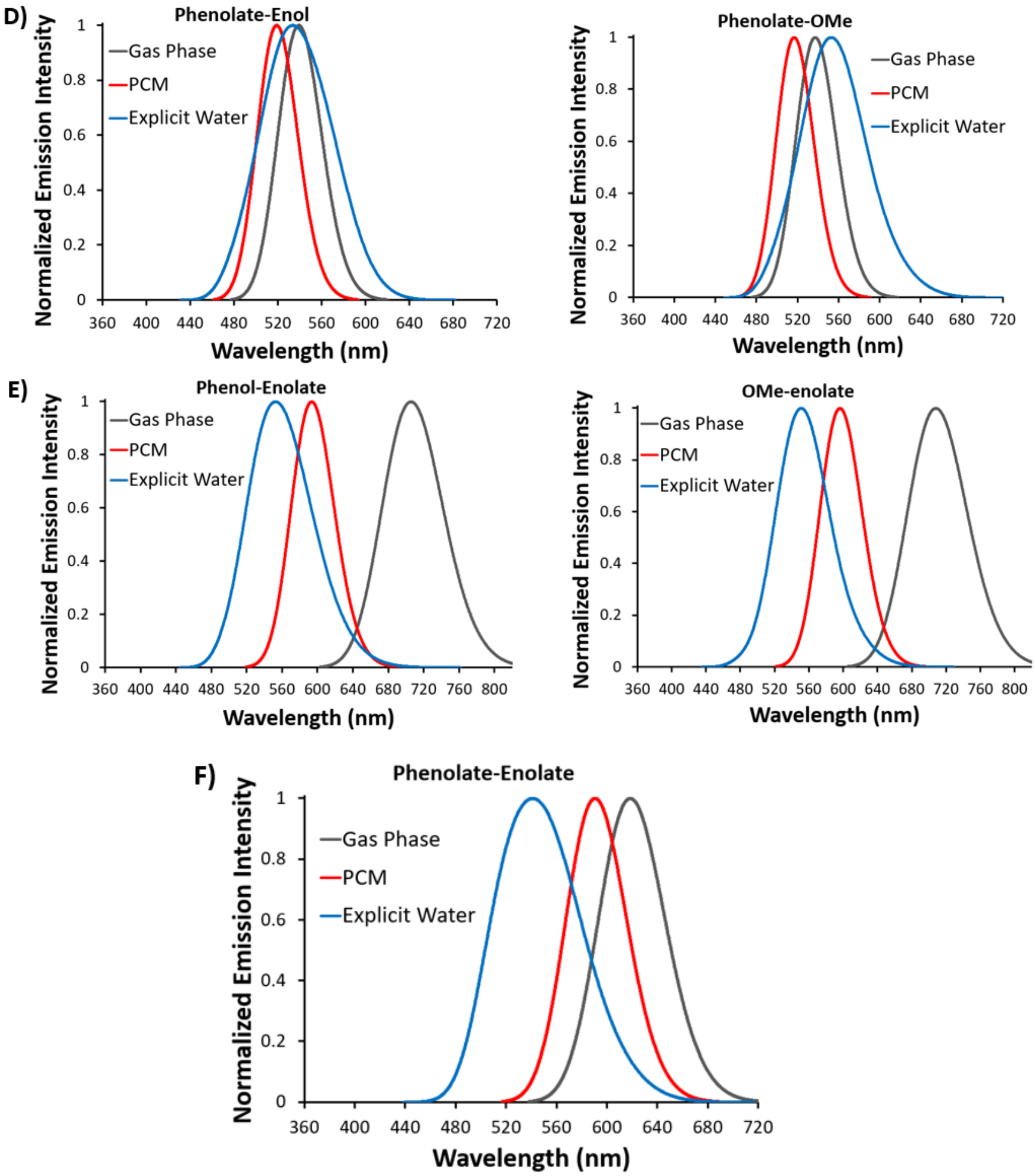

Figure S3. Comparison of the emission spectra computed in the gas phase, within the LR-PCM formalism and QM/MM considering 100 MD snapshots for A) phenol-keto and its analogue, B) phenolate-keto and its analogue, C) phenol-enol and its analogues, D) phenolate-enol and its analogue, E) phenol-enolate and its analogue and F) phenolate-enolate.

7. Vibrationally resolved absorption and emission spectra

The vibrational spectra of phenolate-keto computed with the FC and FCHT approximations are similar, showing only small differences in the band intensity (Figure S3).

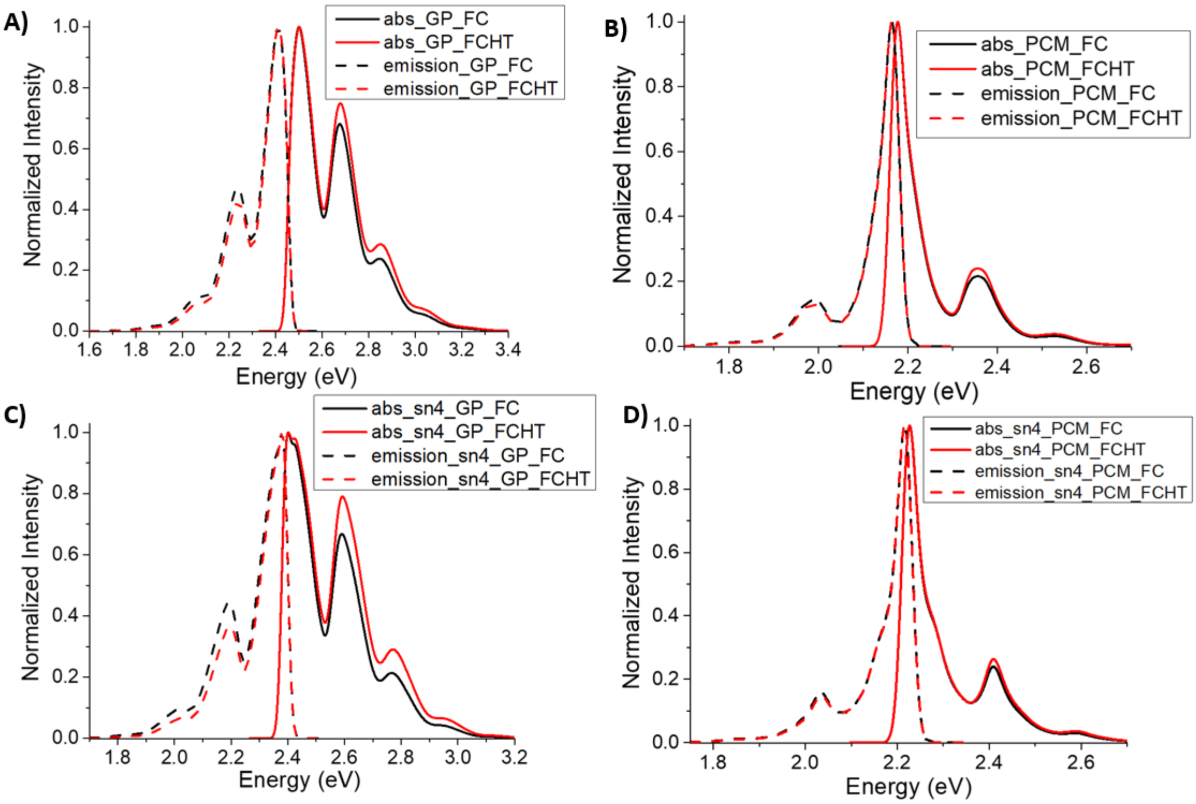

Figure S4. Comparison of the FC and FCHT vibrationally resolved absorption and emission spectra of phenolate keto computed A) in the gas phase, B) with the PCM model, C) with microsolvation in gas phase and D) with microsolvation in PCM.

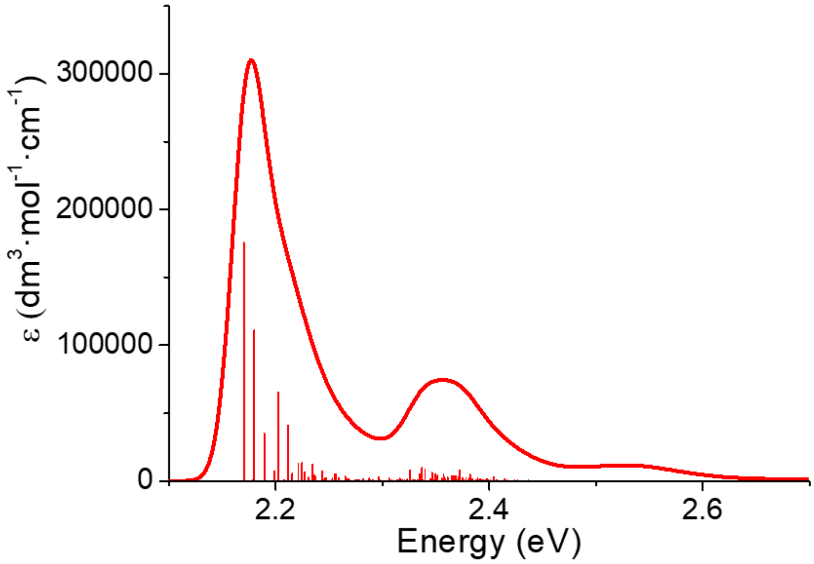

Figure S5. Vibrationally-resolved absorption spectra using the PCM model. Intensity distributions for vibronic transitions are depicted with sticks.

Regarding the microsolvation model, five different snapshots have been selected to compute the vibrationally resolved spectra. Similar absorption and emission spectral shapes have been obtained both in gas phase and with the PCM model. Moreover, the pattern of the most intense vibronic transitions is also similar (Figure S6, S7, S8, S9, S10, S11, S12 and S13). For comparative purposes, the spectra have been shifted to match the maximum of the absorption (2.17743 eV) and emission (2.16355 eV) spectra computed with the PCM model.

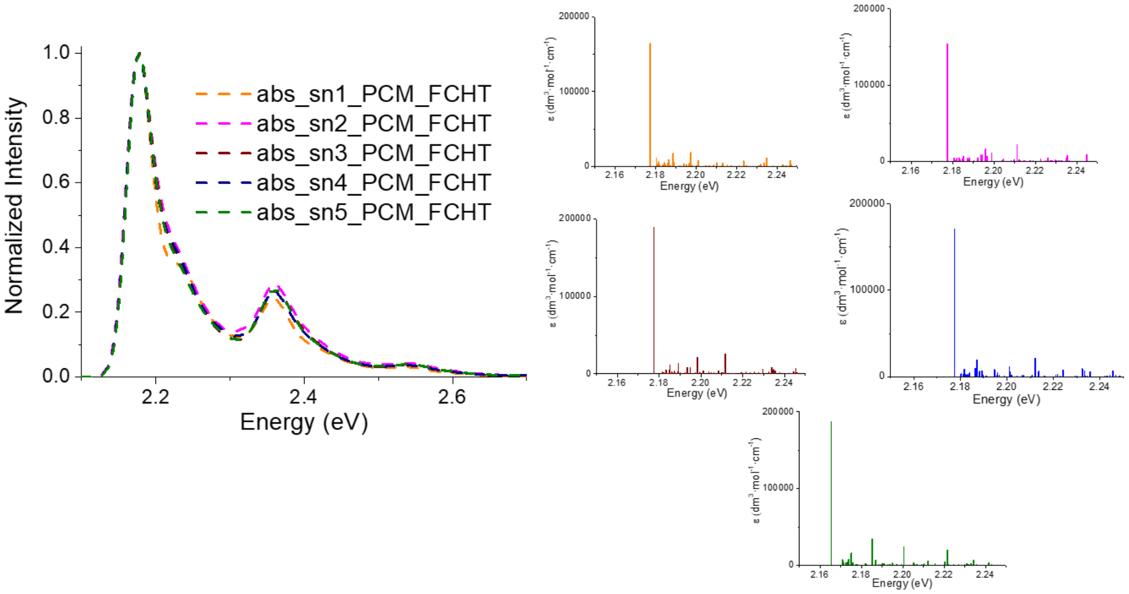

Figure S6. Comparison of the vibrationally resolved absorption spectra of phenolate-keto for the five snapshots used for the microsolvation with the PCM model. The vibronic transitions of the most intense band are depicted as sticks for each snapshot.

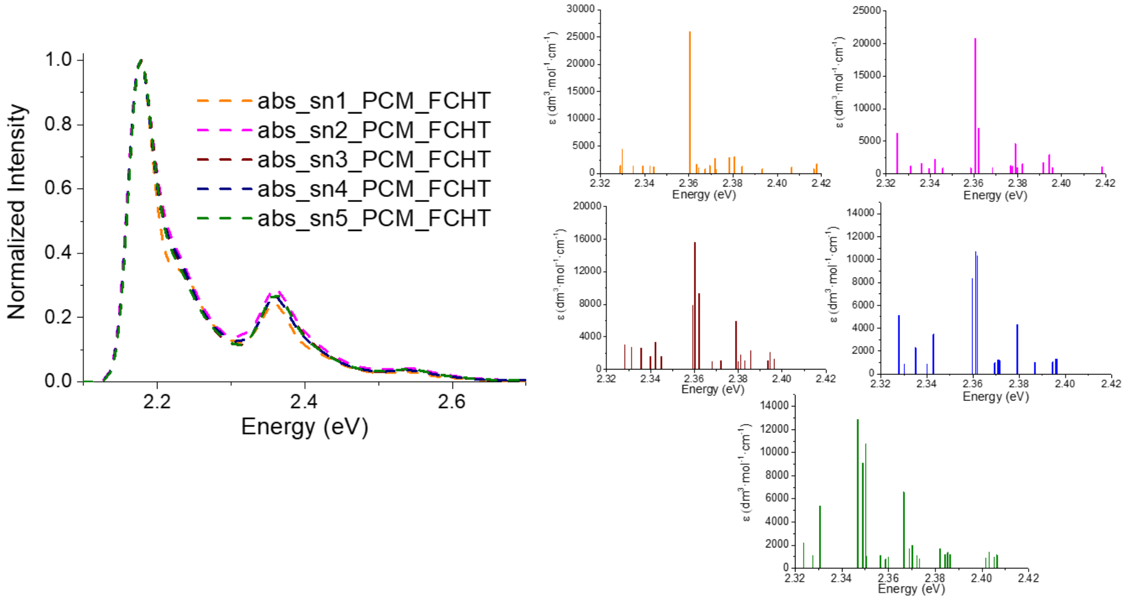

Figure S7. Comparison of the vibrationally resolved absorption spectra of phenolate-keto for the five snapshots used for the microsolvation with the PCM model. The vibronic transitions of the second most intense band are depicted as sticks for each snapshot.

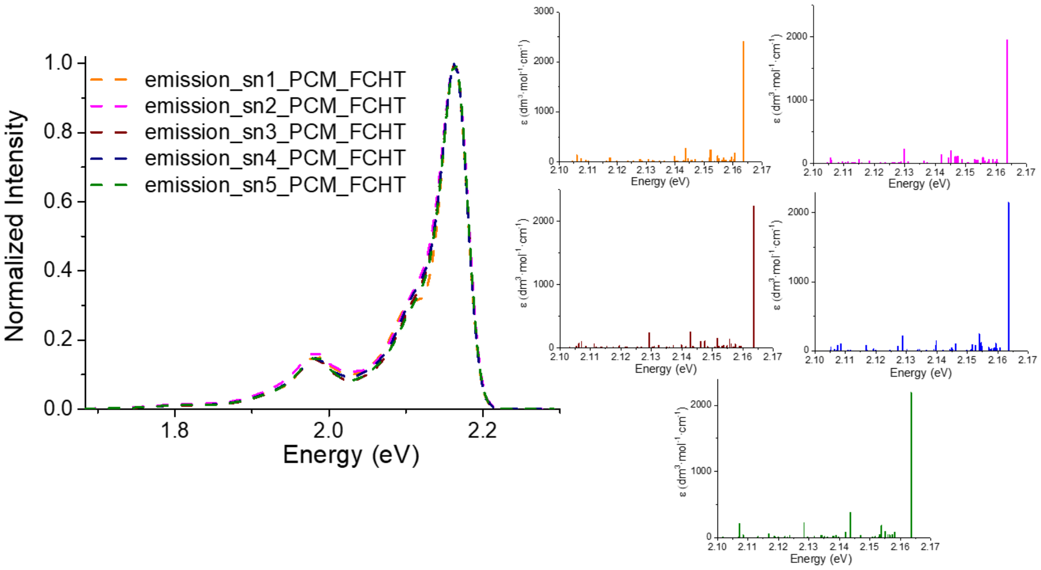

Figure S8. Comparison of the vibrationally resolved emission spectra of phenolate-keto for the five snapshots used for the microsolvation with the PCM model. The vibronic transitions of the most intense band are depicted as sticks for each snapshot.

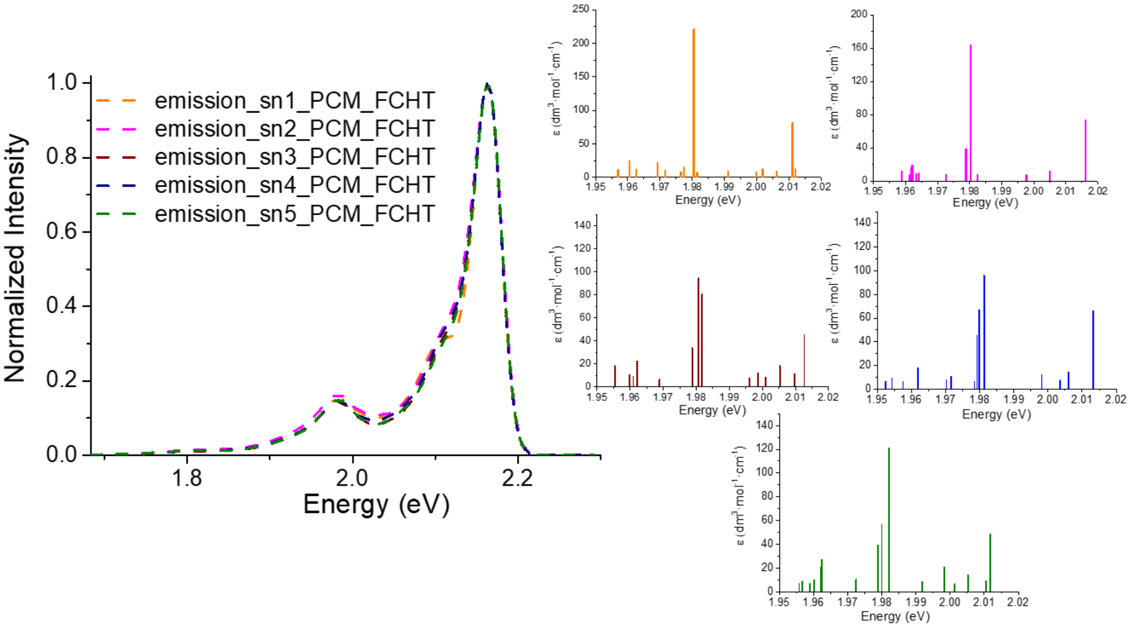

Figure S9. Comparison of the vibrationally resolved emission spectra of phenolate-keto for the five snapshots used for the microsolvation with the PCM model. The vibronic transitions of the second most intense band are depicted as sticks for each snapshot.

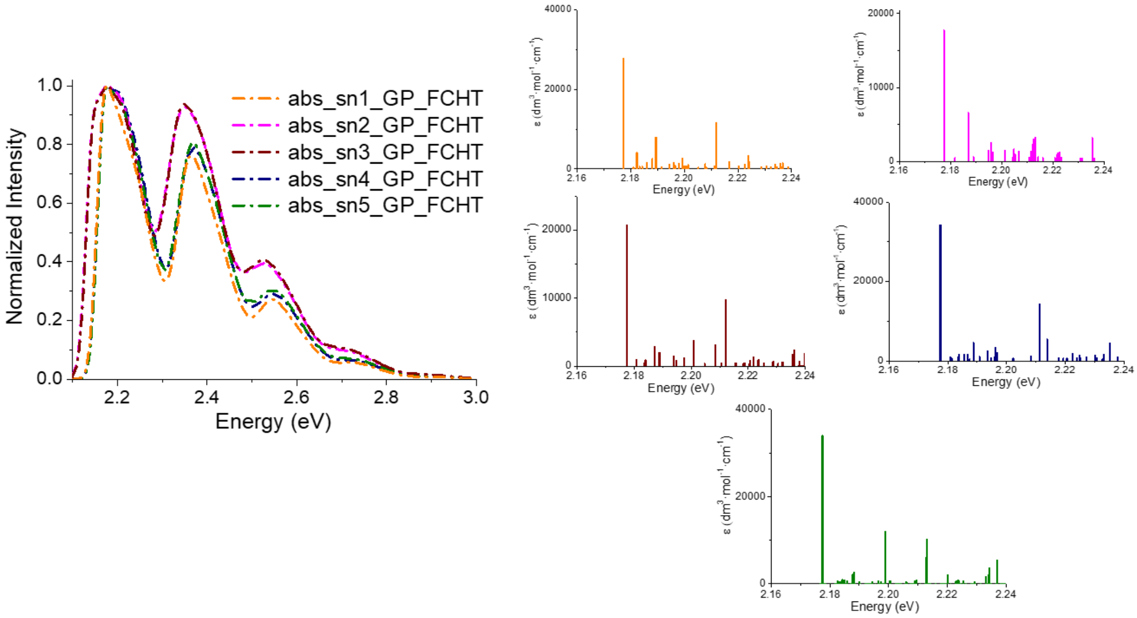

Figure S10. Comparison of the vibrationally resolved absorption spectra of phenolate-keto for the five snapshots used for the microsolvation in gas phase. The vibronic transitions of the most intense band are depicted as sticks for each snapshot.

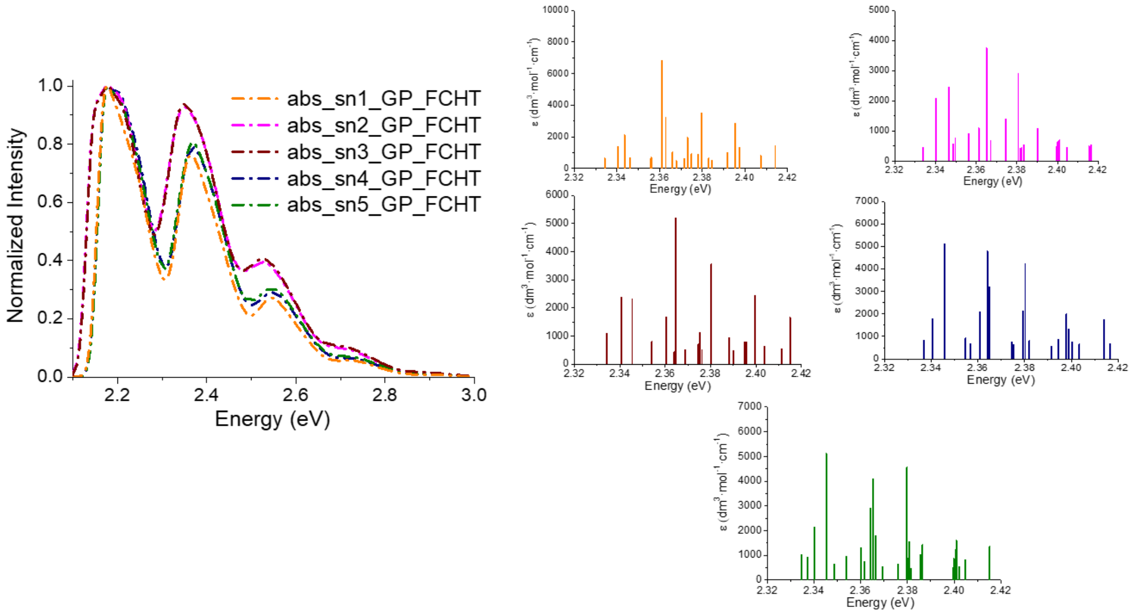

Figure S11. Comparison of the vibrationally resolved absorption spectra of phenolate-keto for the five snapshots used for the microsolvation in gas phase. The vibronic transitions of the second most intense band are depicted as sticks for each snapshot.

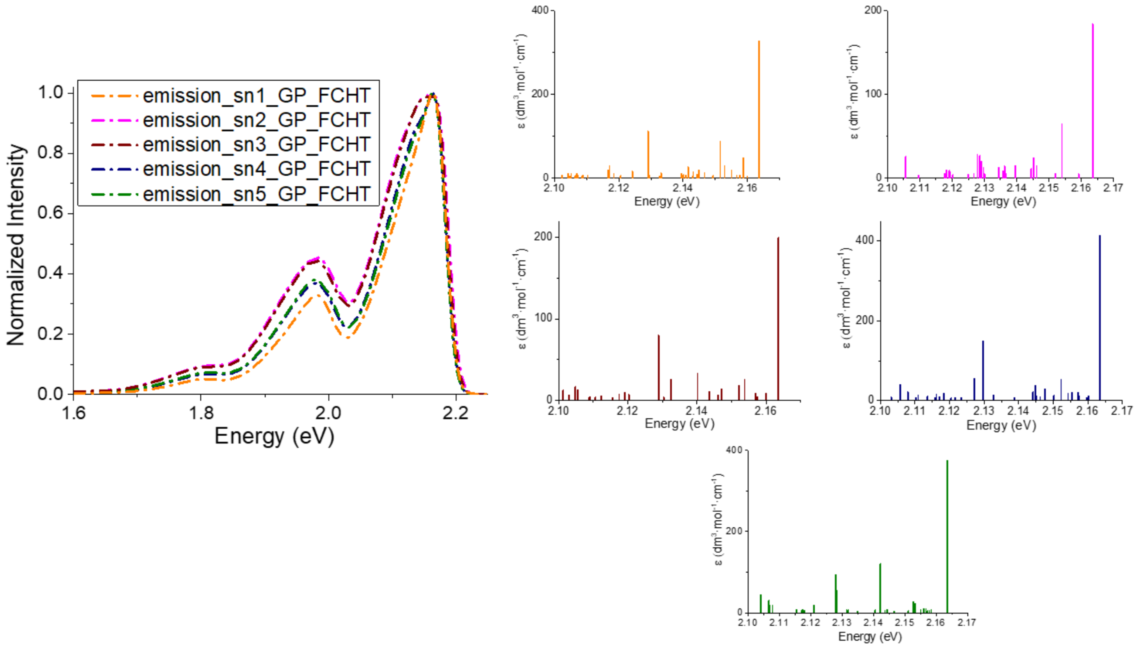

Figure S12. Comparison of the vibrationally resolved emission spectra of phenolate-keto for the five snapshots used for the microsolvation in gas phase. The vibronic transitions of the most intense band are depicted as sticks for each snapshot

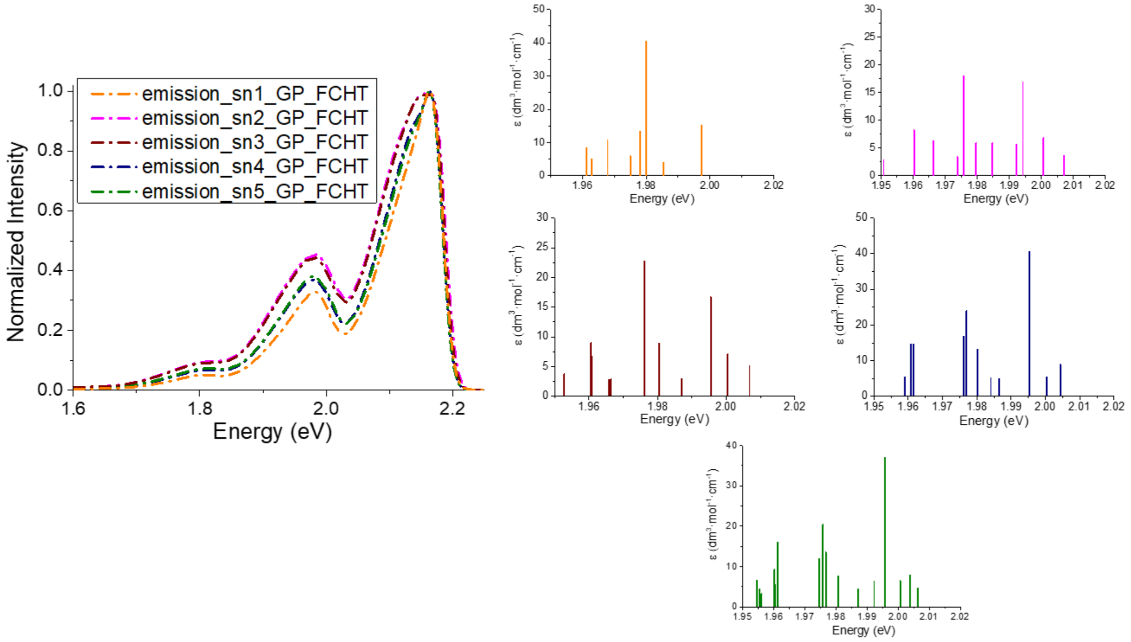

Figure S13. Comparison of the vibrationally resolved emission spectra of phenolate-keto for the five snapshots used for the microsolvation in gas phase. The vibronic transitions of the second most intense band are depicted as sticks for each snapshot.

8. Vibrational modes

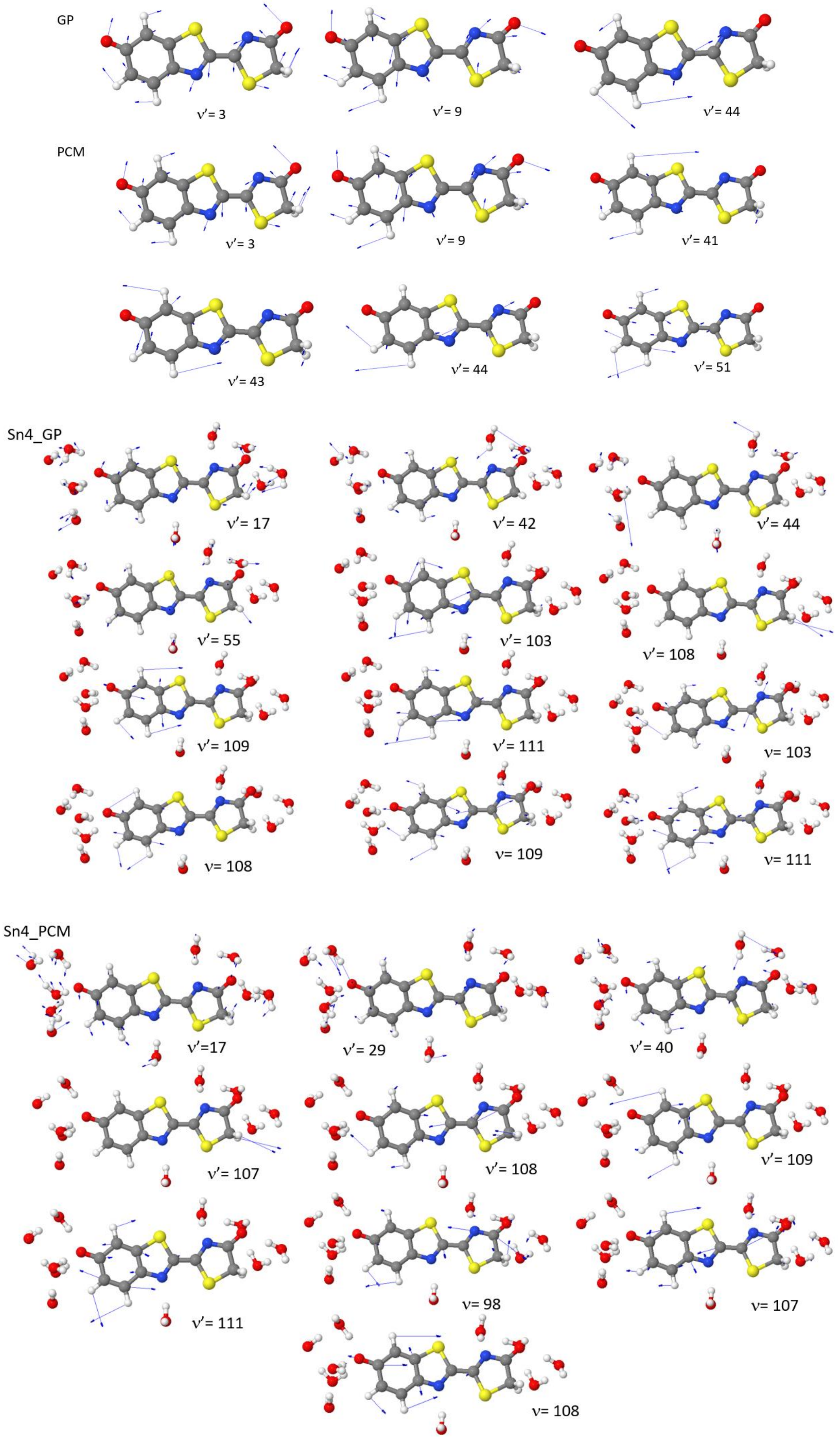

Figure S14. Displacement vectors of the vibrational modes of phenolate-keto detailed in Figures 4 and 5.

(1) Jorgensen, W. L.; Chandrasekhar, J.; Madura, J. D.; Impey, R. W.; Klein, M. L. Comparison of Simple Potential Functions for Simulating Liquid Water. *J. Chem. Phys.* **1983**, *79*, 926–935.

(2) Berendsen, H. J. C.; Postma, J. P. M.; Gunsteren, W. F. van; DiNola, A.; Haak, J. R. Molecular Dynamics with Coupling to an External Bath. *J. Chem. Phys.* **1984**, *81*, 3684.

(3) García-Iriepa, C.; Gosset, P.; Berraud-Pache, R.; Zemmouche, M.; Taupier, G.; Dorkenoo, K. D.; Didier, P.; Léonard, J.; Ferré, N.; Navizet, I. Simulation and Analysis of the Spectroscopic Properties of Oxyluciferin and Its Analogues in Water. *J. Chem. Theory Comput.* **2018**, *14*, 2117–2126.

(4) Ghose, A.; Rebarz, M.; Maltsev, O. V.; Hintermann, L.; Ruckebusch, C.; Fron, E.; Hofkens, J.; Mély, Y.; Naumov, P.; Sliwa, M.; Didier, P. Emission Properties of Oxyluciferin and Its Derivatives in Water: Revealing the Nature of the Emissive Species in Firefly Bioluminescence. *J. Phys. Chem. B* **2015**, *119*, 2638–2649.

(5) Becke, A. Becke's Three Parameter Hybrid Method Using the LYP Correlation Functional. *J. Chem. Phys* **1993**, *98*, 5648–5652.

(6) Lee, C.; Yang, W.; Parr, R. G. Development of the Colle-Salvetti Correlation-Energy Formula into a Functional of the Electron Density. *Phys. Rev. B* **1988**, *37*, 785–789.

(7) Perdew, J. P.; Ernzerhof, M.; Burke, K. Rationale for Mixing Exact Exchange with Density Functional Approximations. *J. Chem. Phys.* **1996**, *105* (22), 9982–9985.

(8) Adamo, C.; Barone, V. Toward Reliable Density Functional Methods without Adjustable Parameters: The PBE0 Model. *J. Chem. Phys.* **1999**, *110* (13), 6158–6170.

(9) Zhao, Y.; Truhlar, D. G. The M06 Suite of Density Functionals for Main Group Thermochemistry, Thermochemical Kinetics, Noncovalent Interactions, Excited States, and Transition Elements: Two New Functionals and Systematic Testing of Four M06-Class Functionals and 12 Other Function. *Theor. Chem. Acc.* **2008**, *120* (1–3), 215–241.

(10) Le Bahers, T.; Adamo, C.; Ciofini, I. A Qualitative Index of Spatial Extent in Charge-Transfer Excitations. *J. Chem. Theory Comput.* **2011**, *7* (8), 2498–2506.

(11) Jacquemin, D.; Bahers, T. Le; Adamo, C.; Ciofini, I. What Is the "Best" Atomic Charge Model to Describe through-Space Charge-Transfer Excitations? *Phys. Chem. Chem. Phys.* **2012**, *14* (16), 5383–5388.

(12) Andrienko, G. http://www.chemcraftprog.com.